Materials Science-Poland
Volume 44 Issue 1 · pp. 50–66 · DOI: 10.2478/msp-2026-0004

Materials Science-Poland

Regulation of microstructural evolution and tribological performance of extruded magnesium matrix composites reinforced with nano-WS_2

Research Article

Zhijian He[1]*, Nengru Tao[2]

[1] *School of Intelligent Manufacturing，Hunan First Normal University, Changsha, China*
[2] *School of Mechanical Engineering, Guangxi University, Nanning, China*

Received 28 January 2026; Accepted 11 March 2026

Abstract: Extruded magnesium matrix composites reinforced with nano-sized tungsten disulfide were fabricated via powder metallurgy followed by hot extrusion, and their microstructural evolution, mechanical response, and tribological behavior were systematically investigated. Compared with monolithic magnesium, the incorporation of 0.5–2.0 wt% nano-reinforcement markedly altered dynamic recrystallization behavior during extrusion, resulting in pronounced grain refinement and texture modification. Electron backscatter diffraction analysis revealed that the average grain size decreased from approximately 8.5 μm in pure magnesium to about 3.2 μm at 2.0 wt% addition, accompanied by a reduction in basal texture intensity from 12.5 to 7.8 m.r.d. These microstructural changes translated into substantial strengthening, with Vickers hardness increasing from 58 to 92 HV0.1, yield strength from 135 MPa to 220 MPa, and ultimate tensile strength from 210 to 315 MPa, while maintaining elongation above 10%. Tribological tests under dry sliding against GCr15 steel demonstrated a pronounced reduction in friction and wear. The steady-state coefficient of friction decreased from ~0.45 for unreinforced magnesium to ~0.18 at 20 N for the composite containing 2.0 wt% reinforcement, and the corresponding wear rate was reduced by nearly one order of magnitude, from $\sim 1.8 \times 10^{-4}$ to $\sim 1.5 \times 10^{-5}$ mm^3 Nm. Surface and debris analyses confirmed the formation of a continuous lubricious tribolayer that mitigated severe adhesive and abrasive wear. The results collectively demonstrate a clear composition–structure–property relationship, highlighting the effectiveness of nanoscale layered reinforcements combined with extrusion processing for achieving a balanced improvement in strength and wear resistance in lightweight metallic composites.

Keywords: *Magnesium matrix composites • Grain refinement • Dynamic recrystallization • Solid lubrication • Wear resistance*

1. Introduction

The escalating demand for lightweight, high-performance materials in the aerospace, automotive, and electronics industries has driven significant research into advanced metallic alloys and composites [1]. Magnesium (Mg) and its alloys have garnered considerable attention as the lightest structural metals, possessing a density approximately two-thirds that of aluminum and one-quarter that of steel [2]. This inherent low density, combined with high specific strength, excellent machinability, and good damping capacity, positions magnesium as a highly attractive material for applications where weight reduction is a critical design criterion [3]. However, the widespread adoption of monolithic magnesium alloys is often hindered by their relatively low elastic modulus, poor ductility, and inferior wear and corrosion resistance, which limit their performance in demanding structural and tribological applications [4,5].

To address these intrinsic limitations, the development of magnesium matrix composites (MMCs) has emerged as a highly effective strategy [6]. By incorporating high-strength, high-stiffness reinforcing phases into the magnesium matrix, MMCs can achieve a synergistic combination of properties unattainable by the individual constituents alone [7]. A diverse range of reinforcements, including ceramic particles (e.g., SiC, Al_2O_3), carbon fibers, and metallic particles, have been investigated to enhance the

* *E-mail: 13080529127@163.com*

mechanical and physical properties of magnesium alloys [8,9]. Among these, nanomaterials have shown exceptional promise due to their unique size-dependent properties and high surface area-to-volume ratio, which can lead to more effective strengthening and functionalization of the composite material [10].

In recent years, two-dimensional (2D) nanomaterials, such as graphene and transition metal dichalcogenides (TMDs), have been explored as novel reinforcements for metal matrix composites. Tungsten disulfide (WS_2), a prominent member of the TMD family, is particularly noteworthy for its excellent solid-lubricating properties, high thermal stability, and good chemical inertness [11]. The unique layered structure of WS_2, with strong covalent bonds within the S–W–S layers and weak van der Waals forces between them, allows for easy interlayer shearing [12]. This intrinsic property makes nano-sized WS_2 an ideal candidate for enhancing the tribological performance of MMCs by reducing the coefficient of friction (COF) and improving wear resistance [13]. The incorporation of nano-WS_2 is expected to form a lubricious tribofilm at the contact interface during sliding, thereby mitigating severe wear mechanisms such as adhesion and abrasion.

Beyond the selection of an appropriate reinforcement, the manufacturing and processing route plays a pivotal role in determining the final microstructure and properties of MMCs [14]. The uniform dispersion of nanoparticles within the metallic matrix remains a significant challenge, as their high surface energy often leads to agglomeration, which can act as stress concentration sites and degrade mechanical performance [15]. Powder metallurgy, stir casting, and various solid-state processing techniques have been employed to fabricate MMCs, each with its own set of advantages and limitations [16]. Among the secondary processing methods, hot extrusion is a widely used and highly effective technique for refining the microstructure of magnesium alloys and their composites [17]. The severe plastic deformation induced during extrusion promotes dynamic recrystallization (DRX), leading to significant grain refinement, homogenization of the microstructure, and elimination of casting defects such as porosity [18]. Furthermore, the extrusion process can help to break up nanoparticle agglomerates and align the reinforcement phase, leading to anisotropic but significantly improved mechanical properties in the extrusion direction [19].

The interplay between nano-WS_2 and hot extrusion is promising, but prior Mg–TMD work has largely emphasized friction reduction without quantitatively resolving extrusion-driven microstructural regulation (DRX kinetics, texture intensity, and their linkage to strengthening and wear) [20]. Specifically, for extruded Mg–WS_2 systems, there is a lack of systematic, composition-resolved evidence connecting nano-WS_2 content to (i) DRX-controlled grain refinement and basal texture weakening quantified by electron backscatter diffraction (EBSD), and (ii) the resulting load-dependent friction/wear response supported by tribolayer chemistry. In addition, the distinction between nano-WS_2 effects and earlier Mg–solid-lubricant composites (e.g., WS_2 or MoS_2 added via powder routes without extrusion-controlled DRX/texture analysis) is not often made quantitatively [21]. To make the distinction from prior Mg solid-lubricant composites explicit, Table 1 summarizes representative quantitative friction/wear metrics for Mg-based composites reinforced with layered solid lubricants (WS_2/MoS_2), together with processing route and test conditions.

The aim of this research is to bridge this knowledge gap by systematically investigating the regulation of microstructural evolution and tribological performance in extruded MMC composites reinforced with varying contents of nano-WS_2. This study focuses on the fabrication of Mg–WS_2 composites via a powder metallurgy route followed by hot extrusion. A comprehensive suite of material characterization techniques, including X-ray diffraction (XRD), scanning electron microscopy (SEM), transmission electron microscopy (TEM), and EBSD, are employed to analyze the phase composition, nanoparticle dispersion, grain structure, and crystallographic texture. The mechanical properties are evaluated through hardness and tensile testing. Finally, the tribological performance is assessed using pin-on-disk wear tests to determine the COF and wear rates, with a detailed analysis of the underlying wear mechanisms. The findings of this work are expected to provide valuable insights into the design and processing of high-performance, lightweight MMCs for advanced tribological applications.

2. Materials and methods

2.1 Raw materials

The primary matrix material used in this study was high-purity, gas-atomized magnesium powder (99.8% purity, average particle size ~50 µm), supplied by Alfa Aesar. The reinforcement phase consisted of nano-WS_2 powder (99.9% purity, average particle size ~80 nm) from US Research Nanomaterials, Inc. The morphology of the as-received powders was examined using SEM to confirm their size and shape characteristics prior to composite fabrication.

Table 1. Quantitative comparison with representative Mg-based composites reinforced with layered solid lubricants (WS_2/MoS_2).

Matrix/reinforcement	Reinforcement level	Tribo-pair and environment	Test conditions (reported)	Key quantitative tribology metric(s)
Extruded Mg/nano-WS_2	0–2.0 wt%	Pin-on-disk vs GCr15 steel, dry	20 N (also 10, 30 N), 0.1 m s^{-1}, 1,000 m	COF: ~0.45 → ~0.18 (Mg → Mg–2.0WS_2, 20 N). Specific wear rate: ~1.8 × 10^{-4} → ~1.5 × 10^{-5} mm^3 $(N\ m)^{-1}$ (20 N). (This work)
Mg MMCs with WS_2 + SiC	5 wt% WS_2 + 15–20 wt% SiC	Ball-on-disc vs Al_2O_3, polyalphaolefin (PAO) base oil	1–4 N, 22.5 mm s^{-1}; RT & 110°C	Average COF (MMCs): 0.1–0.2 (vs pure Mg 0.16–0.46) [47].
Mg MMC2 (WS_2 + 20 wt % SiC)	5 wt% WS_2 + 20 wt% SiC	Ball-on-disc vs Al_2O_3, PAO oil	RT, 4 N	Wear rate: 0.78 × 10^5 μm^3 $(N\ m)^{-1}$ = 7.8 × 10^{-5} mm^3 $(N\ m)^{-1}$ (reported text) [47].
Mg MMC1 vs MMC2 (WS_2 + SiC)	5 wt% WS_2 + 15–20 wt% SiC	Ball-on-disc vs Al_2O_3, PAO oil	110°C, 4 N	Wear rate: MMC2 2.03 × 10^5 μm^3 $(N\ m)^{-1}$ (=2.03 × 10^{-4} mm^3 $(N\ m)^{-1}$) vs MMC1 3.62 × 10^5 μm^3 $(N\ m)^{-1}$ (=3.62 × 10^{-4} mm^3 $(N\ m)^{-1}$) [47].
AZ31/WS_2 nanotubes	0.1 wt%	Wear test reported (metric via mass loss and depth; COF not tabulated in text)	Conditions not fully quantified in the excerpted text	Wear weight loss: AZ31 1.5608 mg vs AZ31/WS_2 1.035 mg; penetration depth: 170.8 → 143.1 μm with WS_2 nanotubes [48].
Mg/MoS_2 (also Gr)	5–10% (mass fraction)	Pin-on-disc vs EN31 steel, dry	2–15 N, 3.14 m s^{-1}, 2,200 m	Data presented graphically: composites show lower COF than pure Mg, and Mg–10MoS_2 exhibits the lowest COF; wear loss of composites is significantly lower than matrix [49].

2.2 Fabrication of composites

MMCs reinforced with varying weight percentages of nano-WS_2 (0.5, 1.0, 1.5, and 2.0 wt%) were fabricated using a powder metallurgy route followed by hot extrusion. For comparison, a monolithic magnesium sample (0 wt% WS_2) was also prepared under identical processing conditions. The designation for the prepared samples is as follows: Mg (pure magnesium), Mg–0.5WS_2, Mg–1.0WS_2, Mg–1.5WS_2, and Mg–2.0WS_2.

The powder metallurgy process began with the mechanical mixing of magnesium and nano-WS_2 powders. To ensure a homogeneous dispersion of the nanoparticles and prevent agglomeration, a two-step mixing process was employed. First, the required amount of nano-WS_2 powder was dispersed in ethanol and subjected to ultrasonic agitation for 30 min. The magnesium powder was then added to the suspension, and the mixture was mechanically stirred for 1 h, followed by another 30 min of ultrasonication. The resulting slurry was dried in a vacuum oven at 80°C for 12 h to completely evaporate the ethanol. The dried powder mixture was then cold-pressed into cylindrical billets (30 mm in diameter and 40 mm in height) using a uniaxial hydraulic press at a pressure of 500 MPa.

Sintering of the green compacts was carried out in a tube furnace under a protective argon atmosphere. The temperature was ramped up to 600°C at a rate of 10°C min^{-1} and held for 2 h to ensure sufficient densification and metallurgical bonding. After sintering, the billets were allowed to cool to room temperature inside the furnace.

The sintered billets were then subjected to hot extrusion to refine the microstructure and enhance the mechanical properties. Prior to extrusion, the billets were preheated to 350°C for 1 h. The extrusion was performed on a 200 ton horizontal extrusion press with an extrusion ratio of 16:1, at a RAM speed of 1 mm s^{-1}. The die and container were also preheated to 350°C to maintain isothermal conditions. Graphite-based lubricant was applied to the billet surface to reduce friction during extrusion. The final products were cylindrical rods with a diameter of 7.5 mm.

2.3 Mechanical and tribological testing

The mechanical properties of the extruded composites were evaluated by Vickers hardness and tensile tests. The Vickers hardness was measured on the polished cross-section of the samples using a Future-Tech FM-810 microhardness tester with a test force of 0.98 N (equivalent to 100 gf, i.e., 0.1 kgf; reported as HV0.1) and a dwell time of 15 s. At least ten indentations were made for each sample to ensure statistical reliability.

Room temperature tensile tests were performed on a universal testing machine (Instron 5985) according to the ASTM E8 standard. Dog-bone shaped tensile specimens with a gauge length of 25 mm and a diameter of 5 mm were machined from the extruded rods. The tests were conducted at a constant strain rate of 1×10^{-3} s^{-1} until fracture. The yield strength (YS), ultimate tensile strength (UTS), and elongation to failure were determined from the stress–strain curves. At least three specimens were tested for each composite composition to ensure the reproducibility of the results.

The tribological performance of the composites was evaluated using a pin-on-disk tribometer (CSM Instruments) under dry sliding conditions at room temperature, following the principles and reporting framework of ASTM G99 (Wear Testing with a Pin-on-Disk Apparatus), in which a stationary pin/rod specimen slides against a rotating disk under a controlled normal load and sliding speed while friction can be recorded continuously. The composite samples were machined into pins with a diameter of 5 mm and prior to testing, the pin contact faces were prepared using a standardized metallographic procedure (sequential grinding with SiC papers followed by fine polishing) to minimize variability in the running-in stage attributable to surface finish. After preparation, the pins were ultrasonically cleaned in ethanol/acetone and dried in warm air. The initial surface roughness of the pin contact face was measured using a contact profilometer and reported as the arithmetic mean roughness (R_a) (evaluated over multiple traces per specimen); the resulting R_a values were R_a = 0.18 ± 0.03 μm (representative mean value ± standard deviation over five traces per pin) with no statistically meaningful differences among compositions. The counter-disk was made of hardened GCr15 bearing steel with a surface roughness (R_a) of approximately 0.1 μm.

The wear tests were conducted at a sliding speed of 0.1 m s^{-1} for a total sliding distance of 1,000 m, under applied normal loads of 10, 20, and 30 N. For each material–load condition, the tribological test was repeated three times using freshly prepared pins and a new wear track region on the counter-disk to ensure statistical reliability. The COF was continuously recorded during the tests, and the reported friction coefficients and wear rates represent the mean value with the associated scatter (±standard deviation) obtained from the repeated measurements. The wear loss of the pins was first quantified by mass loss (Δm) using a microbalance with an accuracy of 0.01 mg. The mass loss was then converted to volumetric wear loss using the experimentally measured density of each extruded material, i.e., $\Delta V = \Delta m/\rho$, where ρ is the density (g cm^{-3}) determined by the Archimedes method (ethanol as immersion medium, room temperature; $n = 3$ per composition). The measured densities were 1.732 ± 0.004 g cm^{-3} for Mg, 1.739 ± 0.005 g cm^{-3} for Mg–0.5WS_2, 1.746 ± 0.004 g cm^{-3} for Mg–1.0WS_2, 1.753 ± 0.005 g cm^{-3} for Mg–1.5WS_2, and 1.760 ± 0.006 g cm^{-3} for Mg–2.0WS_2. These experimentally measured densities, rather than theoretical values, were used for all mass-to-volume conversions in the wear-rate calculation. The specific wear rate was calculated as $K = \Delta V/(F{\cdot}L)$ and reported in mm^3 N^{-1} m^{-1}, where F is the applied normal load and L is the total sliding distance. This procedure follows standard pin-on-disk reporting practice when wear is measured by mass loss. The worn surfaces of the pins and the wear debris were subsequently examined by SEM and energydispersive X-ray spectroscopy (EDS) to identify the active wear mechanisms. In addition, X-ray photoelectron spectroscopy (XPS) was employed on selected wear tracks to confirm the presence of W/S-containing tribospecies and to elucidate tribochemical products formed during sliding.

2.4 Phase and microstructural characterization (XRD)

Phase identification of the as-received WS_2 powder, extruded pure Mg, and extruded Mg–WS_2 composites was performed by XRD using a diffractometer equipped with a Cu Kα radiation source (λ = 1.5406 Å) operated at 40 kV and 40 mA. Diffraction patterns were collected over 2θ = 10°–80° with a step size of 0.02° and a scanning rate of 2° min^{-1}. To enable peak-shape analysis, selected Mg reflections were fitted using a pseudo-Voigt function after background subtraction, and the instrumental contribution to peak broadening was accounted for using a standard reference (measured under identical conditions). The full width at half maximum (FWHM) values were then used to evaluate broadening trends and to estimate the relative contributions of crystallite size and microstrain using a Williamson–Hall-type approach.

3. Results and discussion

3.1 Microstructural characterization

The phase composition of the as-received nano-WS_2 and Mg–WS_2 composites was analyzed by XRD, and the resulting patterns are shown in Figure 1 with the principal reflections indexed. The pure extruded Mg sample shows the characteristic peaks of hexagonal close-packed (HCP) Mg (JCPDS 35-0821), where the major reflections can be assigned to (100), (002), (101), (102), (110), and (103) planes. The as-received WS_2 powder exhibits the characteristic peaks of hexagonal 2H-WS_2 (JCPDS 08-0237), including the prominent (002) reflection at ~14.3° and higher-angle peaks that can be indexed to (004), (100), (101), (103), (006), and (110).

In the Mg–WS_2 composites, Mg reflections remain dominant, while WS_2 peaks become progressively more detectable with increasing reinforcement fraction, consistent with the increased phase fraction. No additional peaks attributable to interfacial reaction products (e.g., Mg–S compounds or W-containing intermetallics) were observed within the XRD detection limit, indicating that the selected powder-metallurgy plus extrusion route preserved the chemical identity of WS_2 under the present processing window. Beyond phase identification, we examined Mg peak positions and peak widths to probe lattice-level changes. Any Mg peak-position variations across compositions were small (within the angular resolution of our instrument under the reported step size) and did not indicate a systematic, composition-driven lattice-parameter change; nevertheless, such peak-position changes, when present, are commonly associated with elastic strains from residual stress or lattice distortion introduced by plastic deformation and thermal-mismatch constraints in composites [22].

In contrast, a modest but consistent broadening tendency of selected Mg reflections was observed with increasing WS_2 content after peak fitting, reflected by increased FWHM values. Since diffraction peak broadening can arise from reduced coherently diffracting domain size and increased microstrain (e.g., dislocation density/microstress), we added an FWHM-based analysis (Williamson–Hall-type treatment) to provide crystallite-size/microstrain insight complementary to the EBSD grain-size trends (noting that XRD crystallite size represents coherent domain size and need not equal EBSD grain size) [23]. We summarize the fitted peak-position and FWHM values in a supplementary table (Table S1).

The dispersion of the nano-WS_2 reinforcement and the overall microstructure of the extruded composites were examined using SEM and TEM. Figure 2 shows the SEM micrographs of the longitudinal sections of the extruded pure Mg and the Mg–WS_2 composites. The pure Mg sample exhibits a refined and elongated grain structure, which is characteristic of hot-extruded magnesium alloys. The grains are aligned along the extrusion direction, a result of the severe plastic deformation and DRX that occurred during the extrusion process [22].

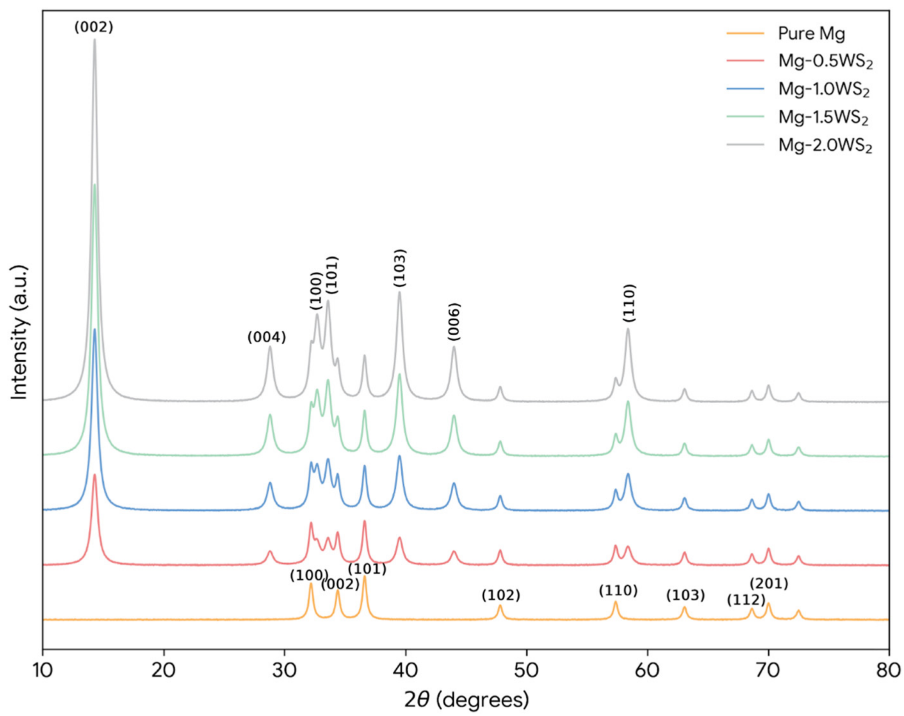

Figure 1. XRD patterns of the extruded pure Mg and Mg–WS_2 composites.

In the Mg–WS_2 composites, the nano-WS_2 particles are generally well-dispersed within the magnesium matrix, although some small agglomerates are still visible, particularly at higher reinforcement contents (e.g., Mg–2.0WS_2). The presence of the nanoparticles has a significant influence on the microstructure. It is evident that the addition of nano-WS_2 leads to a more refined grain structure compared to the monolithic Mg. This grain refinement effect can be attributed to two main mechanisms [24]. First, the WS_2 nanoparticles can act as nucleation sites for new grains during DRX. Second, the nanoparticles can exert a pinning effect on the grain boundaries (Zener pinning), which restricts their growth after recrystallization. This effect becomes more pronounced with increasing WS_2 content, leading to a progressively finer grain size.

To further investigate the distribution of the reinforcement and the interfacial characteristics, EDS mapping and high-magnification SEM were performed, as shown in Figure 3. The EDS maps for W and S elements confirm the presence and distribution of the WS_2 nanoparticles within the magnesium matrix. The maps indicate a relatively uniform distribution of the reinforcement, which is crucial for achieving consistent mechanical properties. At higher magnifications, it can be observed that the WS_2 nanoparticles are located both at the grain boundaries and within the grain interiors [25–27]. The particles situated at the grain boundaries are particularly effective in hindering grain growth.

TEM analysis was conducted to provide a more detailed view of the nanoparticle–matrix interface and the dislocation structures. Figure 4 presents a bright-field TEM image of the Mg–1.5WS_2 composite. The image reveals a high density of dislocations within the magnesium matrix, which is a consequence of the severe plastic deformation during extrusion [28]. The nano-WS_2 particles are clearly visible and are well-bonded to the matrix. The interface between the WS_2 nanoparticles and the Mg matrix appears to be clean and sharp, with no evidence of any interfacial reaction products or voids [29]. This good interfacial bonding is essential for effective load transfer from the matrix to the reinforcement, which is a key factor for the strengthening of the composite [30–32]. The interaction between the dislocations and the nanoparticles is also evident, as the dislocations can be seen to be pinned by the WS_2 particles [33]. This interaction contributes to the dislocation strengthening of the composite.

To quantitatively analyze the grain structure and crystallographic texture of the extruded composites, EBSD analysis was performed. Figure 5 displays the inverse pole figure (IPF) maps of the pure Mg and the Mg–WS_2 composites. The maps visually confirm the grain refinement effect of the nano-WS_2 addition. The average grain size of the pure Mg was measured to be approximately 8.5 μm. In contrast, the average grain size of the composites decreased progressively with increasing WS_2 content, reaching a minimum of approximately 3.2 μm for the

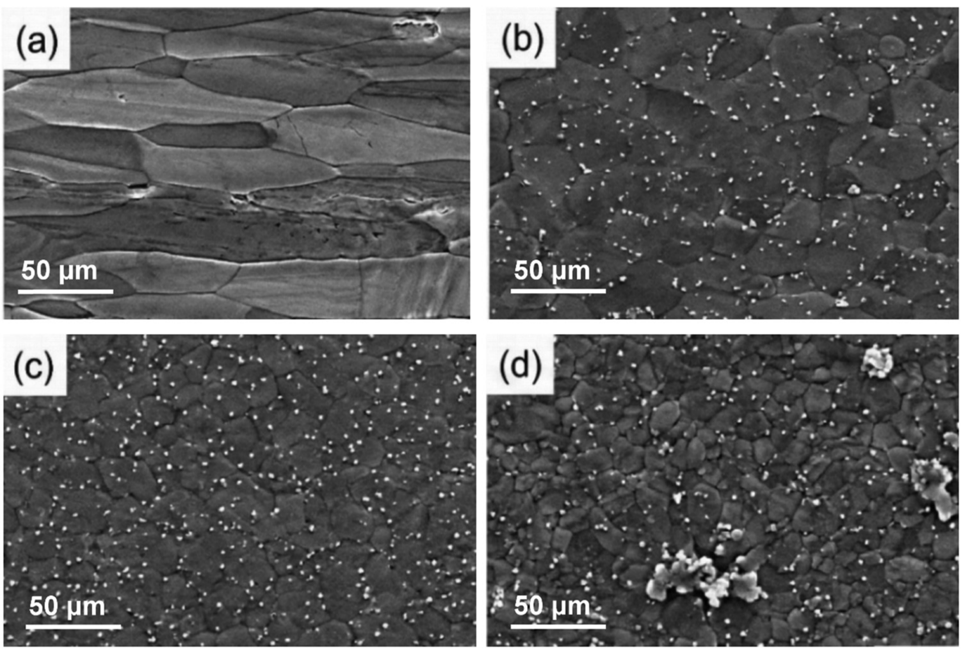

Figure 2. SEM micrographs of the extruded (a) pure Mg, (b) Mg–0.5WS_2, (c) Mg–1.0WS_2, and (d) Mg–2.0WS_2 composites.

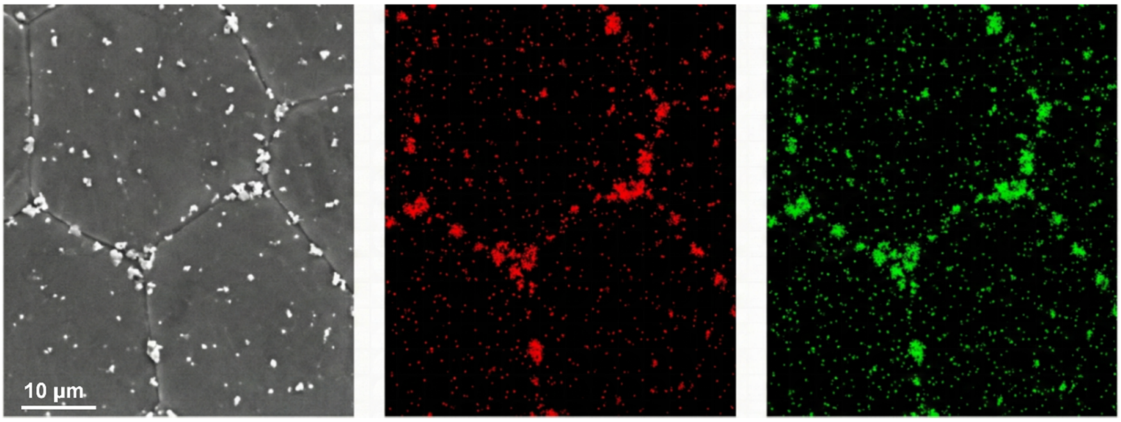

Figure 3. High-magnification SEM image and corresponding EDS elemental maps of the Mg–1.5WS_2 composite, showing the distribution of W and S.

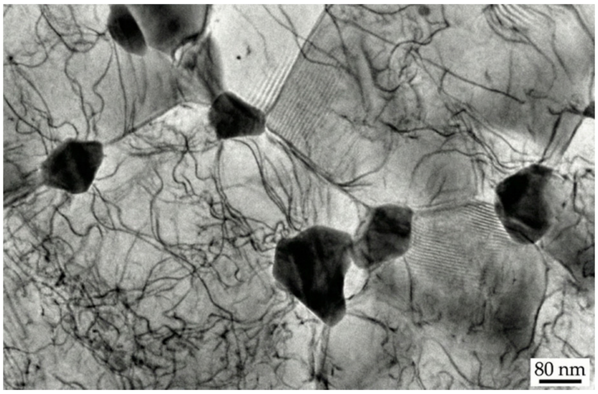

Figure 4. TEM micrograph of the Mg–1.5WS_2 composite, revealing the nanoscale features of the reinforcement and the matrix.

Mg–2.0WS_2 composite. This represents a grain size reduction of over 60% compared to the unreinforced matrix, highlighting the potent role of nano-WS_2 particles in inhibiting grain growth during DRX.

The grain size distribution histograms, also presented in Figure 5, show a shift toward smaller grain sizes and a narrower distribution as the WS_2 content increases. This indicates a more homogeneous and refined microstructure in the composites with higher reinforcement loading. The fine and uniform grain structure is expected to contribute significantly to the improvement of the mechanical properties of the composites according to the Hall–Petch relationship.

The hot extrusion process typically induces a strong crystallographic texture in magnesium alloys. Figure 6 shows the (0001) pole figures for the extruded pure Mg and the Mg–WS_2 composites. All samples exhibit a typical basal texture, where the (0001) basal planes of the HCP crystal structure are preferentially aligned parallel to the extrusion direction. This is a common feature in extruded magnesium alloys and is responsible for the anisotropic mechanical behavior. However, the intensity of the basal texture is observed to be weakened with the addition of nano-WS_2. The maximum texture intensity decreases from 12.5 m.r.d. (multiples of random distribution) for pure Mg to 7.8 m.r.d. for the Mg–2.0WS_2 composite. This texture weakening effect can be attributed to the influence of nanoparticles on the DRX process. The presence of the WS_2 particles can promote the nucleation of new grains with more random orientations, a phenomenon known as particle-stimulated nucleation [34]. This randomization of the texture can be beneficial for improving the ductility and formability of the composites.

3.2 Mechanical properties

The mechanical properties of the extruded pure Mg and Mg–WS_2 composites were evaluated in terms of Vickers

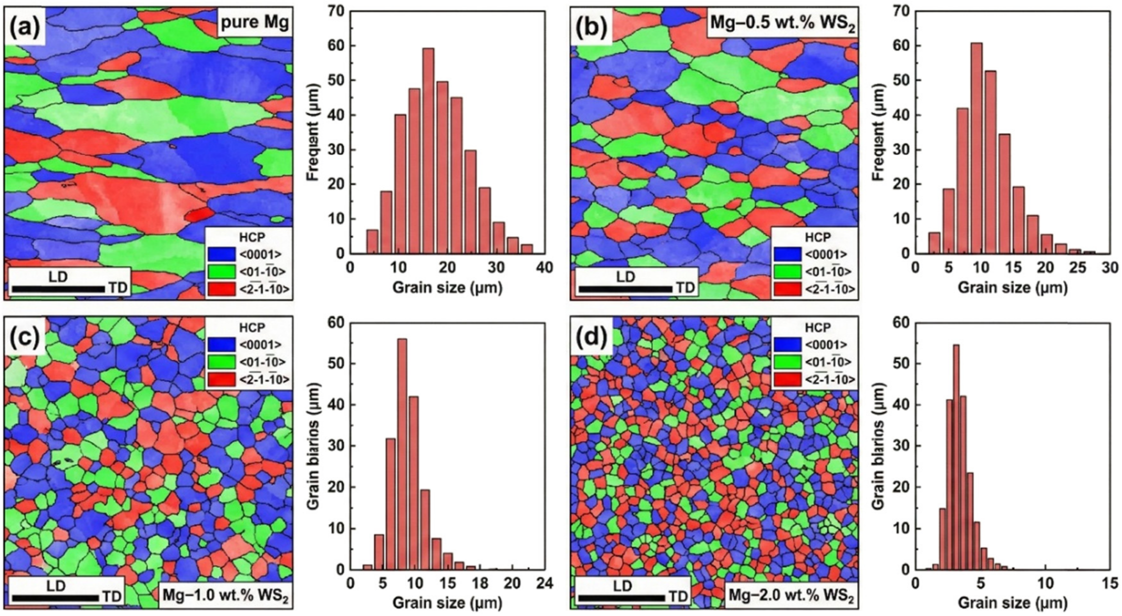

Figure 5. EBSD IPF maps and corresponding grain size distribution histograms for (a) pure Mg, (b) Mg–0.5WS_2, (c) Mg–1.0WS_2, and (d) Mg–2.0WS_2 composites.

hardness and room temperature tensile properties. The results are summarized in Table 2, and the representative tensile stress–strain curves are shown in Figure 7. The Vickers hardness of the composites is observed to increase significantly with the addition of nano-WS_2. The pure Mg sample has a hardness of 58 HV0.1, while the hardness of the Mg–2.0WS_2 composite reaches 92 HV0.1, representing an improvement of approximately 59%. This substantial increase in hardness can be attributed to several factors. The primary reason is the presence of the hard WS_2 nanoparticles, which act as obstacles to the movement of dislocations. Additionally, the significant grain refinement

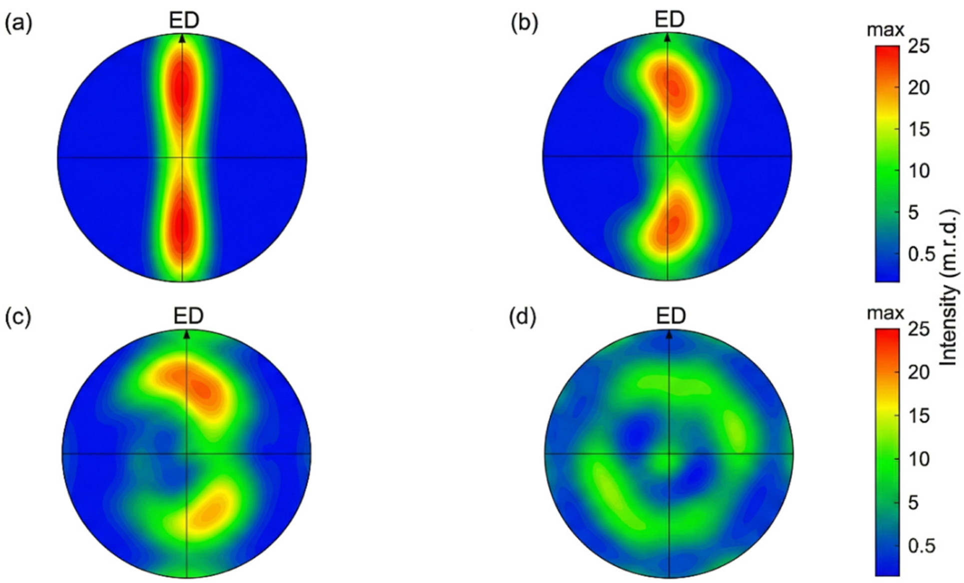

Figure 6. (0001) pole figures of the extruded (a) pure Mg, (b) Mg–0.5WS_2, (c) Mg–1.0WS_2, and (d) Mg–2.0WS_2 composites, showing the texture evolution.

Material	Vickers hardness (HV0.1)	YS (MPa)	UTS (MPa)	Elongation to failure (%)
Pure Mg	58 ± 3	135 ± 5	210 ± 8	18.5 ± 1.2
Mg–0.5WS_2	68 ± 4	160 ± 6	245 ± 7	16.2 ± 1.0
Mg–1.0WS_2	76 ± 4	185 ± 5	275 ± 9	14.8 ± 0.9
Mg–1.5WS_2	85 ± 5	205 ± 7	300 ± 10	12.5 ± 0.8
Mg–2.0WS_2	92 ± 5	220 ± 8	315 ± 11	10.3 ± 0.7

Table 2. Mechanical properties of the extruded pure Mg and Mg–WS_2 composites.

achieved in the composites, as confirmed by the EBSD analysis, contributes to the increased hardness according to the Hall–Petch effect. The high density of dislocations generated during the extrusion process also plays a role in the overall hardness improvement.

The tensile properties of the composites also show a marked improvement with the addition of nano-WS_2. As seen from the stress–strain curves in Figure 7, both the YS and UTS increase progressively with increasing WS_2 content. The YS of the pure Mg is 135 MPa, which increases to 220 MPa for the Mg–2.0WS_2 composite (a 63% improvement). Similarly, the UTS increases from 210 MPa for pure Mg to 315 MPa for Mg–2.0WS_2 (a 50% improvement). This significant strengthening is a result of the combined effects of several strengthening mechanisms, including:

1. Grain boundary strengthening (Hall–Petch effect): The refinement of the grain size leads to an increase in the volume fraction of grain boundaries, which act as barriers to dislocation motion.
2. Orowan strengthening: The nano-WS_2 particles dispersed in the matrix act as obstacles to the movement of dislocations, which have to bow out between the particles, leading to an increase in the stress required for deformation.
3. Load transfer strengthening: The load is effectively transferred from the softer magnesium matrix to the harder WS_2 reinforcement, which carries a larger portion of the applied load.
4. Dislocation strengthening: The high density of dislocations generated during extrusion and due to the thermal mismatch between the matrix and the reinforcement contributes to the overall strength.

However, the enhancement in strength is accompanied by a decrease in ductility. The elongation to failure decreases from 18.5% for pure Mg to 10.3% for the Mg–2.0WS_2 composite. This trade-off between strength and ductility is commonly observed in metal matrix composites [35]. The presence of the hard ceramic nanoparticles can limit the plastic deformation of the matrix and act as potential sites for crack initiation, especially where agglomerates are present [36]. Nevertheless, the composites still retain a reasonable level of ductility, which is important for structural applications.

3.3 Tribological performance

The tribological behavior of the extruded pure Mg and Mg–WS_2 composites was investigated under dry sliding conditions against a GCr15 steel counter-disk. Figure 8 shows the variation in the COF as a function of sliding distance for the different materials tested under a normal load of 20 N. For all samples, the COF exhibits an initial running-in period, characterized by some fluctuations, after which it stabilizes to a relatively steady-state value [37]. The pure Mg sample shows the highest COF, with a steady-state value of approximately 0.45. This is attributed to the severe adhesive wear and plastic deformation that occurs at the contact surface [36].

With the addition of nano-WS_2, the COF of the composites is significantly reduced. The steady-state COF decreases progressively with increasing WS_2 content, reaching a minimum of approximately 0.18 for the Mg–2.0WS_2 composite. This represents a reduction of about 60% compared to the pure Mg. This remarkable improvement in the frictional behavior is a direct consequence of the solid-lubricating effect of the WS_2 nanoparticles. During sliding, WS_2 can be mechanically exposed and smeared into the contact, participating in the development of a low-shear transfer layer/tribolayer that reduces the real area of metal-to-metal junctions and suppresses adhesive plucking. In the present work, the progressive COF decrease with increasing WS_2 content together with the markedly smoother wear-track morphology at high WS_2 loading supports the presence of a lubricious third-body layer; however, because cross-sectional tribolayer analysis and full-area wear-track EDS mapping were not performed, we describe this feature conservatively as a WS_2-assisted tribolayer rather than asserting a compositionally verified "WS_2-rich tribofilm." This interpretation aligns with prior reports on WS_2-containing Mg composites and WS_2 tribofilm formation routes, where low-friction behavior is attributed to transfer-film generation and shear within layered WS_2-containing tribophases.

To directly verify the chemical signature of this tribolayer, XPS was performed on representative wear tracks (pure Mg and Mg–2.0WS_2, tested at 20 N). High-resolution spectra (Figure S1) show the characteristic W 4f doublet

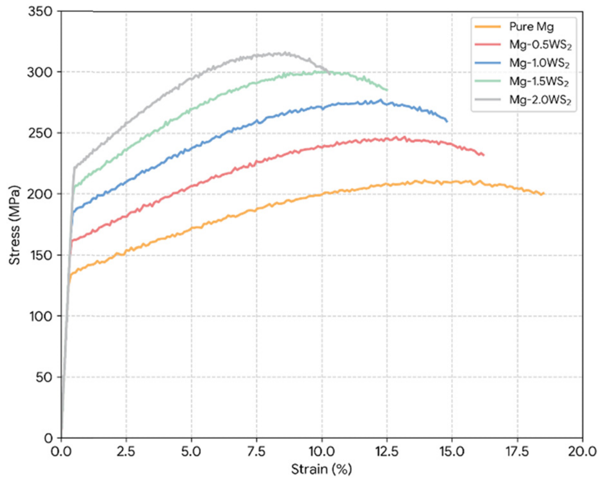

Figure 7. Tensile stress–strain curves of the extruded pure Mg and Mg–WS_2 composites.

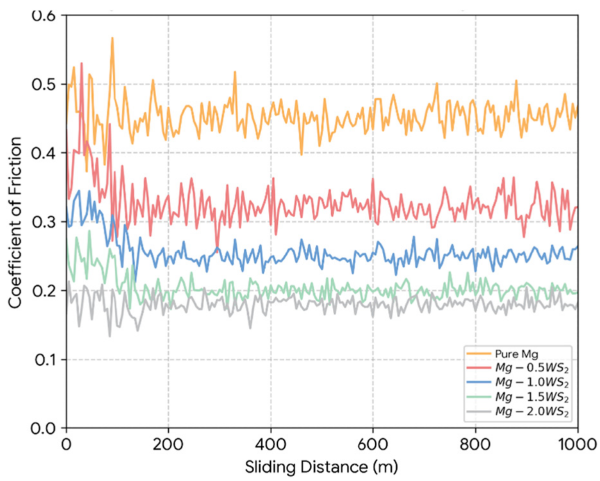

Figure 8. COF as a function of sliding distance for the extruded pure Mg and Mg–WS_2 composites under a normal load of 20 N.

and S 2p doublet attributable to sulfide species, along with additional oxidized W–O components consistent with partial tribo-oxidation of WS_2 during sliding. The Mg 2p/O 1s envelopes indicate a mixed MgO/$Mg(OH)_2$ contribution, suggesting that the W/S-bearing tribolayer forms within an oxide/hydroxide-containing tribochemical matrix. These XPS results provide direct compositional evidence that the wear-track surface is enriched in W/S-containing species, supporting the proposed transfer-layer mechanism for friction and wear reduction. Similar use of wear-track XPS to confirm chalcogenide-derived tribofilms has been widely reported for WS_2-containing self-lubricating composites and related TMD tribosystems.

The effect of the applied normal load on the steady-state COF is presented in Table 3. For all materials, the COF tends to decrease slightly with increasing normal load. This behavior can be attributed to the increased contact area and the formation of a more stable and compacted tribolayer at higher loads [38]. This trend is consistent with load-assisted compaction of third-body debris and tribochemical products into a more load-bearing interfacial layer, which can reduce metal-to-metal junction growth and stabilize sliding. However, film compaction under higher load does not necessarily imply film integrity; higher shear stresses can also promote local cracking and delamination. To directly assess load-induced changes in layer continuity and damage, representative SEM–EDS analyses of worn surfaces at the highest load (30 N) (Figure S2) are performed, enabling a microstructure-supported interpretation of the load-dependent wear mechanism.

Material	COF (10 N)	COF (20 N)	COF (30 N)
Pure Mg	0.48 ± 0.03	0.45 ± 0.02	0.42 ± 0.02
Mg–0.5WS_2	0.35 ± 0.02	0.32 ± 0.02	0.30 ± 0.01
Mg–1.0WS_2	0.28 ± 0.02	0.25 ± 0.01	0.23 ± 0.01
Mg–1.5WS_2	0.22 ± 0.01	0.20 ± 0.01	0.18 ± 0.01
Mg–2.0WS_2	0.20 ± 0.01	0.18 ± 0.01	0.16 ± 0.01

Table 3. Steady-state COF of the extruded pure Mg and Mg–WS_2 composites at different normal loads.

The specific wear rates of the extruded pure Mg and Mg–WS_2 composites were calculated from mass-loss measurements by converting Δm to wear volume ($\Delta V = \Delta m/\rho$) using the experimentally measured density for each composition, and the results are presented in Figure 9 and summarized in Table 4. The wear rate of the pure Mg is significantly high, especially under higher normal loads, which is consistent with its poor wear resistance. The addition of nano-WS_2 leads to a dramatic reduction in the wear rate of the composites. For instance, under a normal load of 20 N, the wear rate of the Mg–2.0WS_2 composite is approximately 1.5×10^{-5} mm^3 $(N\ m)^{-1}$, which is about an order of magnitude lower than that of the pure Mg (1.8×10^{-4} mm^3 $(N\ m)^{-1}$).

This substantial improvement in wear resistance is directly linked to the enhanced mechanical properties (hardness and strength) of the composites and the effective lubrication provided by the WS_2 nanoparticles. The harder composite matrix is more resistant to plastic deformation and ploughing by the asperities of the steel counter-disk [38]. More importantly, the improved wear resistance at higher WS_2 contents is consistent with the formation of a more stable protective tribolayer/transfer film, which reduces direct junction growth and limits severe adhesion while also diminishing abrasive ploughing by providing a lower-shear interfacial medium. In similar WS_2-containing tribosystems, such layers are commonly confirmed by SEM/EDS and/or XPS as W/S-bearing tribophases that evolve during sliding; accordingly, we interpret our friction–wear trends and surface morphologies as indirect but coherent evidence of tribolayer-assisted protection under the present test conditions [39]. The wear rate is observed to decrease systematically with increasing WS_2 content, which correlates with the lower friction coefficients and the formation of a more robust and continuous lubricating film.

The effect of the normal load on the wear rate is also significant. For all materials, the wear rate increases with increasing normal load, as expected. The rate of increase is substantially lower for the WS_2-containing composites, implying that a WS_2-assisted third-body/tribochemical layer continues to provide partial interfacial protection at elevated contact pressures. In the original version, this point was inferred primarily from friction–wear trends; in the revision, we provide direct worn-surface microstructural evidence at 30 N (Figure S2) showing that the transfer/tribolayer becomes more compact but may exhibit localized cracking and partial delamination under higher load. This interpretation is consistent with classic load-driven transitions in film-controlled wear, where protective layers can be stabilized by compaction yet simultaneously challenged by accelerated removal at higher load.

To understand the underlying wear mechanisms, the worn surfaces of the composite pins were examined using

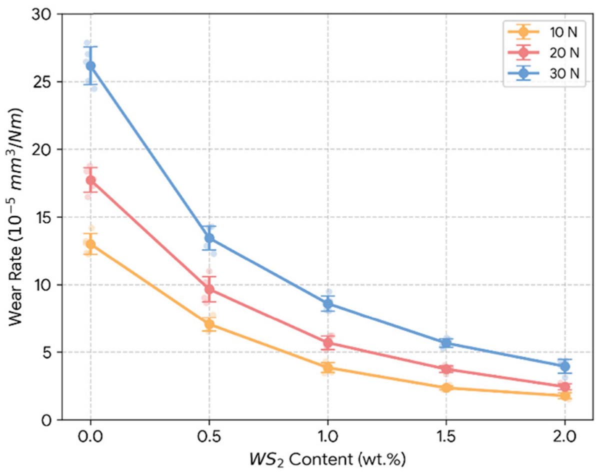

Figure 9. Wear rates of the extruded pure Mg and Mg–WS_2 composites as a function of WS_2 content at different normal loads.

Material	Wear rate (10 N) ($\times10^{-5}$ mm^3 (N m)$^{-1}$)	Wear rate (20 N) ($\times10^{-5}$ mm^3 (N m)$^{-1}$)	Wear rate (30 N) ($\times10^{-5}$ mm^3 (N m)$^{-1}$)
Pure Mg	12.5 ± 1.1	18.2 ± 1.5	25.8 ± 2.0
Mg–0.5WS_2	6.8 ± 0.6	9.5 ± 0.8	13.2 ± 1.1
Mg–1.0WS_2	4.2 ± 0.4	6.1 ± 0.5	8.9 ± 0.7
Mg–1.5WS_2	2.5 ± 0.2	3.8 ± 0.3	5.5 ± 0.4
Mg–2.0WS_2	1.8 ± 0.2	2.5 ± 0.2	3.9 ± 0.3

Table 4. Wear rates of the extruded pure Mg and Mg–WS_2 composites at different normal loads.

SEM and EDS. Figure 10a and b shows the SEM micrographs of the worn surfaces of the pure Mg and the Mg–2.0WS_2 composite after sliding under a normal load of 20 N.

The worn surface of the pure Mg (Figure 10a) is characterized by severe plastic deformation, deep grooves parallel to the sliding direction, and evidence of extensive adhesive wear. This indicates that the dominant wear mechanisms are abrasion and adhesion. The soft magnesium matrix is easily ploughed by the hard asperities of the steel counter-disk, leading to the formation of grooves and the generation of large, metallic wear debris. The high friction and localized temperature rise at the contact points also promote strong adhesion between the surfaces, resulting in material transfer and delamination.

In stark contrast, the worn surface of the Mg–2.0WS_2 composite (Figure 10b) is much smoother and exhibits significantly less damage. The deep grooves and severe plastic deformation seen on the pure Mg surface are absent. Given the monotonic improvement in COF and wear rate with WS_2 addition (Tables 3 and 4), we additionally include representative worn-surface SEM images for intermediate compositions (Mg–1.0WS_2 and Mg–1.5WS_2) in the Figure 10c and d. These images illustrate a clear progression in wear features with reinforcement content: (i) pure Mg shows deep grooves, severe plastic flow, and adhesive delamination characteristic of mixed

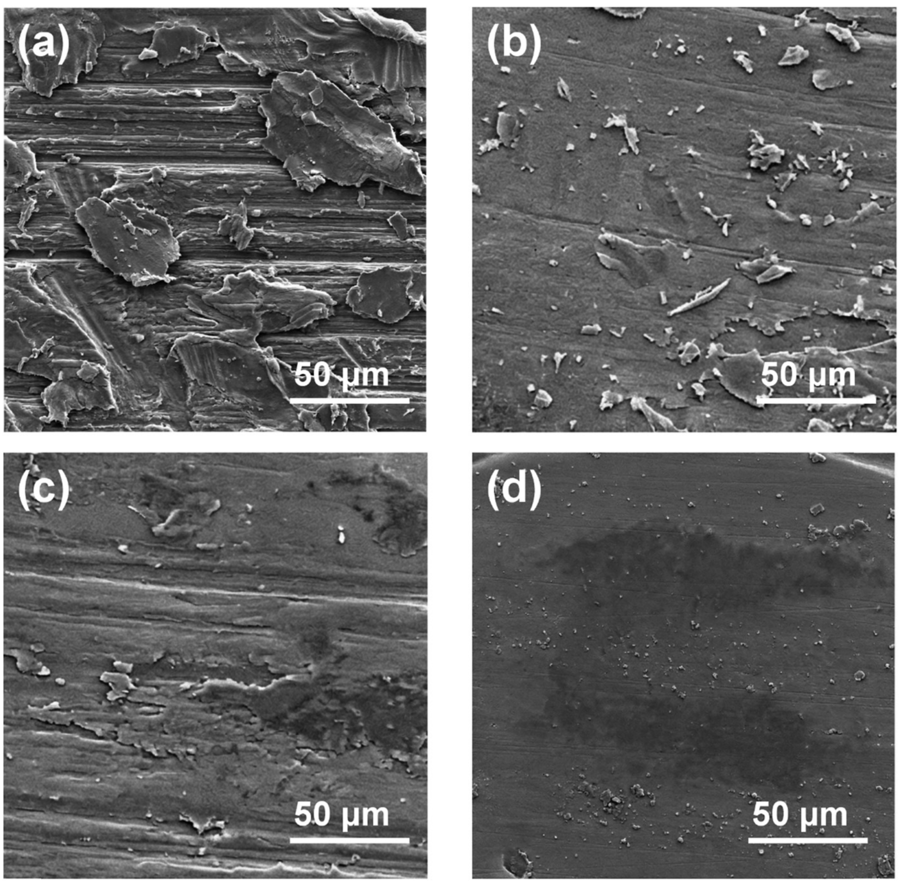

Figure 10. SEM micrographs of worn surfaces after dry sliding under a load of 20 N: (a) pure Mg, (b) Mg–1.0WS_2, (c) Mg–1.5WS_2, and (d) Mg–2.0WS_2 composites.

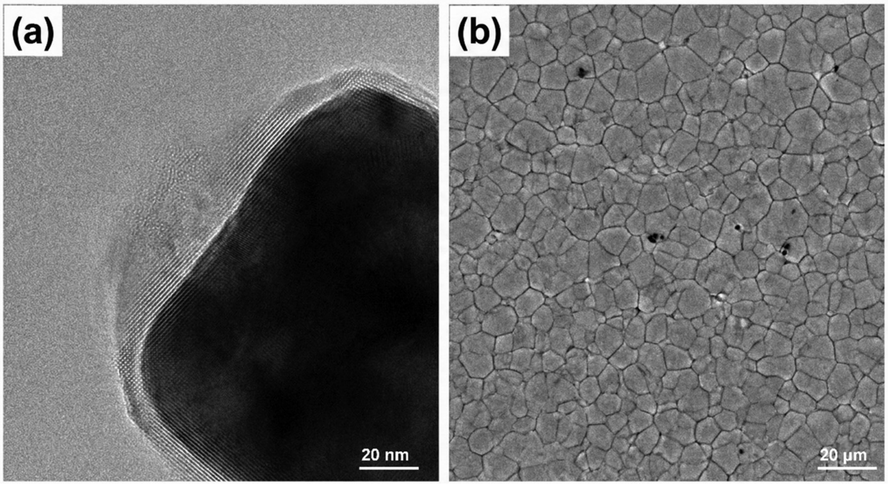

Figure 11. (a) High-resolution micrograph showing the clean and well-bonded interface between a WS_2 nanoparticle and the Mg matrix. (b) Micrograph illustrating the refined and equiaxed grain structure in the Mg–1.0WS_2 composite.

abrasive–adhesive wear; (ii) intermediate WS_2 contents show reduced groove depth and fewer large delamination patches, indicating suppression of severe adhesion and a transition toward milder abrasion with increasing surface coverage by compacted debris/tribolayer fragments; and (iii) Mg–2.0WS_2 exhibits the smoothest track with the most extensive compacted surface layer, where wear is dominated by mild abrasion and tribolayer delamination in localized regions rather than bulk adhesive tearing. This composition-dependent transition is consistent with the general third-body framework for solid-lubricant-containing MMCs, in which increasing lubricant supply promotes a more continuous shear layer and reduces counterface attack. The primary wear mechanism for the composites appears to be a mild abrasive and oxidative wear, with some evidence of delamination of the tribolayer in localized regions [40]. Relative to prior Mg–(WS_2/MoS_2) solid-lubricant composites that primarily report friction/wear trends, the present work advances the state of the art by quantitatively linking nano-WS_2 content to extrusion-controlled DRX and texture evolution (EBSD-derived grain size and basal texture intensity) and then to load-dependent friction and wear. This microstructure-resolved pathway explains why the best tribological performance coincides with the most refined grains and weakened basal texture, while XPS-confirmed W/S-bearing tribospecies provide chemical evidence that the friction reduction is not solely a hardness effect but also a third-body/tribolayer mechanism.

Material	Average grain size (μm)	Texture index (m.r.d.)
Pure Mg	8.5 ± 0.7	12.5
Mg–0.5WS_2	6.8 ± 0.5	10.9
Mg–1.0WS_2	5.2 ± 0.4	9.3
Mg–1.5WS_2	4.1 ± 0.3	8.1
Mg–2.0WS_2	3.2 ± 0.3	7.8

Table 5. Summary of EBSD results for the extruded pure Mg and Mg–WS_2 composites.

3.4 Interfacial analysis

The nature of the interface between the reinforcement and the matrix is critical to the overall performance of a metal matrix composite, as it governs the efficiency of load transfer and can influence fracture behavior. To further scrutinize the interfacial region between the nano-WS_2 particles and the Mg matrix, detailed SEM and TEM examinations were conducted. Figure 11a provides a high-resolution view of the interface in the Mg–1.5WS_2 composite.

The micrograph clearly shows an intimate and well-bonded interface between a WS_2 nanoparticle and the surrounding Mg matrix. There is no evidence of voids, debonding, or the presence of a significant reaction layer at the interface [41]. This clean and coherent interface is crucial for ensuring that the load applied to the composite is effectively transferred from the relatively soft matrix to the much harder and stiffer reinforcement particles [42]. The absence of a brittle interfacial reaction product is particularly important, as such phases can act as crack initiation sites and compromise the ductility and toughness of the composite [43]. The successful fabrication via the powder metallurgy and hot extrusion route at controlled temperatures has effectively prevented significant chemical reactions between the thermodynamically reactive Mg and the WS_2 particles [44].

The strong interfacial bonding also plays a role in the observed strengthening. During deformation, a strong interface prevents premature failure by nanoparticle pull-out and allows for the development of other strengthening mechanisms, such as Orowan looping and the generation of a high dislocation density in the matrix surrounding the particles due to thermal expansion mismatch [45]. The slight lattice mismatch between the Mg matrix and the WS_2 particles can induce localized strain fields at the interface, which can further impede dislocation motion and contribute to the overall strength of the composite [46].

Figure 11b provides another perspective on the refined grain structure achieved in the composites. The image highlights the equiaxed and homogeneous nature of the recrystallized grains in the Mg–1.0WS_2 composite. The uniform distribution of these fine grains is a direct result of the DRX process being influenced by the dispersed nanoparticles. This refined microstructure is not only beneficial for strength and hardness but also contributes to the improved tribological performance by providing a more uniform and stable substrate for the formation of the protective tribofilm.

Table 5 summarizes the key microstructural parameters obtained from the EBSD analysis, quantitatively illustrating the impact of nano-WS_2 addition on the grain structure and texture of the extruded composites. The data clearly show the progressive grain refinement and texture weakening with increasing reinforcement content, which are key factors contributing to the observed improvements in mechanical properties.

4. Conclusion

In this study, MMCs reinforced with varying contents of nano-WS_2 (0.5, 1.0, 1.5, and 2.0 wt%) were successfully fabricated by a powder metallurgy route followed by hot extrusion. The influence of the nano-WS_2 reinforcement on the microstructural evolution, mechanical properties, and tribological performance of the extruded composites was systematically investigated. Based on the comprehensive experimental results, the following conclusions can be drawn:

1. The addition of nano-WS_2 particles to the magnesium matrix resulted in significant grain refinement. The average grain size of the composites decreased from 8.5 μm for pure Mg to 3.2 μm for the Mg–2.0WS_2 composite. This grain refinement is attributed to the pinning effect of the nanoparticles on the grain boundaries and their role as nucleation sites during DRX.
2. The nano-WS_2 particles were found to be well-dispersed within the magnesium matrix, with a clean and coherent interface, indicating good interfacial bonding. The hot extrusion process also led to a weakening of the basal texture in the composites compared to the monolithic Mg, which is beneficial for improving the isotropy of the material.
3. The mechanical properties of the composites were significantly enhanced by the addition of nano-WS_2. The Vickers hardness, YS, and UTS of the Mg–2.0WS_2 composite improved by approximately 59, 63, and 50%, respectively, compared to pure Mg. This strengthening is a result of the combined effects of grain refinement, Orowan strengthening, and effective load transfer.
4. The tribological performance of the composites was remarkably improved. The COF and the wear rate of the Mg–2.0WS_2 composite were reduced by up to 60% and an order of magnitude, respectively, compared to the unreinforced Mg. This is attributed to the formation of a protective W/S-containing tribolayer/transfer film on the worn surface, which acts as a low-shear solid-lubricating third body; wear-track XPS confirms the presence of W- and S-bearing species (with partial tribo-oxidation products), consistent with a transition from severe adhesive–abrasive wear toward a milder tribochemical wear regime.

In summary, this research demonstrates that the incorporation of nano-WS_2 is a highly effective strategy for simultaneously enhancing the mechanical and tribological properties of extruded magnesium composites. The tailored microstructure, characterized by a refined grain structure and a well-dispersed reinforcement phase, leads to a superior combination of strength, hardness, and wear resistance. These findings suggest that Mg–WS_2 nanocomposites have great potential for application in lightweight, high-performance components subjected to tribological loading conditions

Funding information

Authors state no funding involved.

Author contributions

Z.H. contributed to conceptualization, methodology, investigation, formal analysis, data curation, visualization, and writing the original draft. N.T. contributed to methodology, validation, formal analysis, writing review and editing, supervision, and project administration. Z.H. and N.T. contributed to data interpretation and approved the final version of the manuscript. All authors have read and agreed to the published version of the manuscript.

Conflict of interest statement

The authors declare no conflicts of interest to report regarding the present study.

Data availability statement

The data that support the findings of this study are available from the corresponding author upon reasonable request.

References

[1] Singhal, V., Shelly, D., Babbar, A., Lee, S.Y., Park, S.J. Review of wear and mechanical characteristics of Al-Si alloy matrix composites reinforced with natural minerals. Lubricants. 2024;12(10):350

[2] Hu, S., Wang, F., Du, X., Mao, P., Wang, Z., Zhou, L., et al. Microstructure, mechanical properties and wear resistance of As-Cast Mg–3Al-1Ca-0.4 Mn/Tip magnesium matrix composites. Int. J. Metalcast. 2025;19(3):1422–1437

[3] Wang, H., Luo, X.C., Zhang, D.T., Qiu, C., Chen, D.L. High-strength extruded magnesium alloys: A critical review. J. Mater. Sci. Technol. 2024;199:27–52. doi: 10.1016/j.jmst.2024.01.089

[4] Sagar, P., Handa, A., Kumar, G. Metallurgical, mechanical and tribological behavior of reinforced magnesium-based composite developed via friction stir processing. Proc. Inst. Mech. Eng., Part. E: J. Process. Mech. Eng. 2022;236(4):1440–1451

[5] Patel, S.K., Singh, S., Shi, L., Liu, L., Zhang, X., Guan, L., et al. Microstructural and biological wear behaviour of hybrid reinforced AZ91D alloy surface composite fabricated by friction stir processing technique. Ceram. Int. 2025; 51: 64337–64354. doi: 10.1016/j.ceramint.2025.11.171

[6] Rajoria, S.R., Kanti, S.P., Soni, H., Sahoo, B.N. Development, characterization, and mechanical properties of innovative *in situ* high-entropy alloy reinforced magnesium matrix composites *via* ultrasonic-assisted processing. J. Manuf. Process. 2025;142:368–386. doi: 10.1016/j.jmapro.2025.03.094

[7] Ren, J.Y., Ji, G.C., Guo, H.R., Zhou, Y.M., Tan, X., Zheng, W.F., et al. Nano-enhanced phase reinforced magnesium matrix composites: A review of the matrix, reinforcement, interface design, properties and potential applications. Materials. 2024;17(10):2454. doi: 10.3390/ma17102454

[8] Sahoo, S., Sahoo, B., Panigrahi, S. Investigation into machining performance of microstructurally engineered in-situ particle reinforced magnesium matrix composite. J. Magnes. Alloy. 2023;11(3):916–935

[9] Bharathi, P., Sampath Kumar, T. Latest research and developments of ceramic reinforced magnesium matrix composites—A comprehensive review. Proc. Inst. Mech. Eng., Part. E: J. Process. Mech. Eng. 2023;237(3):1014–1035

[10] Aliasker, K., Gopal, P., Naveen, S., Madhu, S., Yuvaraj, K. Exploring the effects of self-lubricating MoS_2 in magnesium metal matrix composite: investigation on wear, corrosion, and mechanical properties. Colloids Surf. A: Physicochem. Eng. Asp. 2023;677:132362

[11] Babu, P., Solomon, D.G. Mechanical and tribological properties of magnesium composites–A review. Mater. Today: Proc. 2023;1:422. doi: 10.1016/j.matpr.2023.07.065

[12] Moradpur-Tari, E., Sarraf-Mamoory, R., Yourdkhani, A. Structural, electronic, and electrochemical studies of WS_2 phases using density functional theory and machine learning. Phys. B: Condens. Matter. 2023;650:414568. doi: 10.1016/j.physb.2022.414568

[13] Ren, G., Wu, X., Cai, W., Gong, P., Chen, Y., Liu, P., et al. WS_2 nanosheet thickness modulation for wear-resistant carbon–graphite composites. Tribol. Int. 2026;214:111359. doi: 10.1016/j.triboint.2025.111359

[14] Zhang, H., Wang, W., Zhang, S., Zhang, Y., Zhou, J., Wang, Z., et al. A novel method based on deep reinforcement learning for machining process route planning. Robot. Comput.-Integr. Manuf. 2024;86:102688. doi: 10.1016/j.rcim.2023.102688

[15] Dey, A., Pandey, K.M. Wear behaviour of Mg alloys and their composites–a review. Int. J. Mater. Res. 2018;109(11):1050–1070

[16] Patel, S.K., Shi, L., Kumar, A., Wu, C., Mironov, S., Zhou, M., et al. A critical review on development of magnesium-based bio-implants surface composite through friction stir processing route. Crit. Rev. Solid. State Mater. Sci. 2025;7:1–86

[17] Li, Q., Zhang, X., Wang, L., Qiao, J. The effect of extrusion and heat treatment on the microstructure and tensile properties of 2024 aluminum alloy. Materials. 2022;15(21):7566. doi: 10.3390/ma15217566
[18] Zhou, H., Ruan, A., Zhang, H., Wang, B., Sun, J., Qin, S., et al. Hot deformation behavior and dynamic recrystallization mechanism of Cr-Co-Ni particle-reinforced AZ31 magnesium matrix composite. J. Alloy. Compd. 2025;1022:179923
[19] Yuan, L., Zheng, B., Kunstmann, J., Brumme, T., Kuc, A.B., Ma, C., et al. Twist-angle-dependent interlayer exciton diffusion in WS_2–WSe_2 heterobilayers. Nat. Mater. 2020;19(6):617–623. doi: 10.1038/s41563-020-0670-3
[20] Zhong, Y., Yue, S., Liang, J., Yuan, L., Xia, Y., Tian, Y., et al. Twist angle-dependent exciton mobility in WS_2 bilayers. Nano Lett. 2025;25(13):5274–5282. doi: 10.1021/acs.nanolett.5c00027
[21] Somveer, Ahlawat, D.S., Singh, D., Gangwar, J. Enhanced structural, morphological and optical properties of WS_2 nanorods synthesized via hydrothermal methodology. Mater. Sci. Eng.: B. 2025;313:117935. doi: 10.1016/j.mseb.2024.117935
[22] Almotairy, S.M., Alharthi, N.H., Alharbi, H.F., Abdo, H.S. Superior mechanical performance of inductively sintered Al/SiC nanocomposites processed by novel milling route. Sci. Rep. 2020;10(1):10368. doi: 10.1038/s41598-020-67198-w
[23] Desai, K.R., Alone, S.T., Wadgane, S.R., Shirsath, S.E., Batoo, K.M., Imran, A., et al. X-ray diffraction based Williamson–Hall analysis and rietveld refinement for strain mechanism in Mg–Mn co-substituted $CdFe_2O_4$ nanoparticles. Phys. B: Condens. Matter. 2021;614:413054. doi: 10.1016/j.physb.2021.413054
[24] Ye, J., Chen, X., Luo, H., Zhao, J., Li, J., Tan, J., et al. Microstructure, mechanical properties and wear resistance of Ti particles reinforced AZ31 magnesium matrix composites. J. Magnes. Alloy. 2022;10(8):2266–2279
[25] Liu, A., Wang, R., Zhang, X., Feng, J., Li, W., Yu, S., et al. On the friction and wear behaviors of a magnesium matrix composite containing 20 vol% Mg_2Sn reinforcement. Tribol. Trans. 2025;13:1–13
[26] Singhal, V., Shelly, D., Saxena, A., Gupta, R., Verma, V.K., Jain, A. Study of the influence of nanoparticle reinforcement on the mechanical and tribological performance of aluminum matrix composites —a review. Lubricants. 2025;13(2):93
[27] Khodabakhshi, F., Simchi, A., Kokabi, A. Surface modifications of an aluminum-magnesium alloy through reactive stir friction processing with titanium oxide nanoparticles for enhanced sliding wear resistance. Surf. Coat. Technol. 2017;309:114–123
[28] Xue, C., Gao, B., Han, T., Che, C., Chu, Z., Tuo, L. Dislocation evolution mechanism of plastic deformation process of AZ31 magnesium alloy with different grain size. Comput. Mater. Sci. 2024;231:112606. doi: 10.1016/j.commatsci.2023.112606
[29] Rahman, M.A., Yomogida, Y., Ahad, A., Ueji, K., Nagano, M., Ihara, A., et al. Synthesis and optical properties of WS_2 nanotubes with relatively small diameters. Sci. Rep. 2023;13(1):16959. doi: 10.1038/s41598-023-44072-z
[30] Vedabouriswaran, G., Aravindan, S. Wear characteristics of friction stir processed magnesium RZ5 composites. J. Tribol. 2019;141(4):041601
[31] Banerjee, S., Sahoo, P., Davim, J.P. Tribological characterisation of magnesium matrix nanocomposites: A review. Adv. Mech. Eng. 2021;13(4):16878140211009025
[32] Aydın, F. Tribological aspects of magnesium matrix composites: A review of recent experimental studies. Tribol.-Mater., Surf. Interfaces. 2023;17(4):363–396
[33] Li, C., Sang, D., Ge, S., Zou, L., Wang, Q. Recent excellent optoelectronic applications based on two-dimensional WS_2 nanomaterials: A review. Molecules. 2024;29(14):3341. doi: 10.3390/molecules29143341
[34] Wang, C.-r., Deng, K.-k. Microstructure, and mechanical and wear properties of Grp/AZ91 magnesium matrix composites. Materials. 2019;12(7):1190
[35] Xia, Y., Zhang, X., Zhao, D., Rong, X., He, C., Zhao, N. Breaking the strength-ductility trade-off for metal matrix composites: A review of the role of nanoscale reinforcement dimension on the deformation and strengthening mechanisms. Rev. Mater. Res. 2025;1(1):100019. doi: 10.1016/j.revmat.2025.100019
[36] Tang, Y., Wang, H., Ouyang, X., Wang, C., Huang, Q., Zhao, Q., et al. Overcoming strength-ductility tradeoff with high pressure thermal treatment. Nat. Commun. 2024;15(1):3932. doi: 10.1038/s41467-024-48435-6
[37] Žemlička, R., Souček, P., Vogl, P., Jílek, M., Buršíková, V., Vašina, P., et al. On the significance of running-in of hard nc-TiC/a-C:H coating for short-term repeating machining. Surf. Coat. Technol. 2017;315:17–23. doi: 10.1016/j.surfcoat.2017.02.020
[38] Gazzato, L., Missale, E., Asnicar, D., Sedona, F., Speranza, G., Del Giudice, A., et al. Structural insights into the mechanical behavior of large-area 2D covalent organic framework nanofilms. ACS Appl. Mater. Interfaces. 2025;17(17):25819–25827. doi: 10.1021/acsami.5c03512

[39] Rodríguez Ripoll, M., Tomala, A.M., Pirker, L., Remškar, M. In-situ formation of MoS_2 and WS_2 tribofilms by the synergy between transition metal oxide nanoparticles and sulphur-containing oil additives. Tribol. Lett. 2020;68(1):41. doi: 10.1007/s11249-020-1286-0

[40] Guo, L., Yin, Y., Gao, L., Lin, H., Liu, Y., Le, K., et al. Tribofilm formation by Fe_3O_4 nanoparticles as lubricant additives: Microscopic insights into growth conditions and mechanisms. Tribol. Lett. 2025;73(2):50. doi: 10.1007/s11249-025-01988-z

[41] Liu, Y., Liu, C.H., Debnath, T., Wang, Y., Pohl, D., Besteiro, L.V., et al. Silver nanoparticle enhanced metal-organic matrix with interface-engineering for efficient photocatalytic hydrogen evolution. Nat. Commun. 2023;14(1):541. doi: 10.1038/s41467-023-35981-8

[42] Nam, J.M., Owen, J.S., Talapin, D.V. The ligand–surface interface and its influence on nanoparticle properties. Acc. Chem. Res. 2023;56(17):2265–2266. doi: 10.1021/acs.accounts.3c00416

[43] Matsuda, T., Hayashi, K., Iwamoto, C., Nozawa, T., Ohata, M., Hirose, A. Crack initiation and propagation behavior of dissimilar interface with intermetallic compound layer in Al/steel joint using coupled multiscale mechanical testing. Mater. Des. 2023;235:112420. doi: 10.1016/j.matdes.2023.112420

[44] Li, B., Chen, H., Li, G., Wei, G., Xie, W. Strengthening and toughening mechanisms of CNTs/Mg–Al composites prepared via powder metallurgy combined with hot extrusion. Vacuum. 2023;214:112210. doi: 10.1016/j.vacuum.2023.112210

[45] Zhang, Y., Nizolek, T.J., Capolungo, L., Li, N., Carpenter, J.S., McCabe, R.J. Strong interfaces: the key to high strength in nano metallic laminates. Acta Mater. 2024;280:120298. doi: 10.1016/j.actamat.2024.120298

[46] Wang, G., Zhang, Y., Liu, J., Chen, W., Wang, K., Cui, B., et al. Dispersion hardening using amorphous nanoparticles deployed via additive manufacturing. Nat. Commun. 2025;16(1):3589. doi: 10.1038/s41467-025-58893-1

[47] Zhu, J., Qi, J., Guan, D., Ma, L., Dwyer-Joyce, R. Tribological behaviour of self-lubricating Mg matrix composites reinforced with silicon carbide and tungsten disulfide. Tribol. Int. 2020;146:106253. doi: 10.1016/j.triboint.2020.106253

[48] Subramani, M., Huang, S.J., Borodianskiy, K. Effect of WS_2 nanotubes on the mechanical and wear behaviors of AZ31 stir casted magnesium metal matrix composites. J. Compos. Sci. 2022;6(7):182. doi: 10.3390/jcs6070182

[49] Narayanasamy, P., Selvakumar, N. Tensile, compressive and wear behaviour of self-lubricating sintered magnesium based composites. Trans. Nonferrous Met. Soc. China. 2017;27(2):312–323. doi: 10.1016/S1003-6326(17)60036-0